ELSEVIER

Journal of Structural Geology 28 (2006) 919–928

JOURNAL OF STRUCTURAL GEOLOGY

www.elsevier.com/locate/jsg

Weakening of deforming granitic rocks with layer development at middle crust

Youngdo Park *,[1], Seung-Hak Yoo [1], Jin-Han Ree

Department of Earth and Environmental Sciences, Korea University, Seoul 136-701, South Korea

Received 28 February 2004; received in revised form 25 January 2006; accepted 5 February 2006
Available online 3 April 2006

Abstract

In the middle crust, deformation of granitic rocks is characterized by crystal plastic deformation of quartz and cataclasis of feldspar. For common granitic rocks with textures of framework feldspar and interstice-filling quartz, brittle strength of feldspar is a close approximation of the bulk rock strength because feldspar forms the load-bearing framework. With deformation, these rocks tend to develop localized high strain zones. The high strain zones commonly consist of quartz-rich layers and feldspar-rich layers. We have examined how the strength of granitic rocks changes with the volume fraction of these layers by combining the flow laws developed by Handy et al. [Handy, M.R., Wissing, S.B., Streit, L.E., 1999. Frictional-viscous flow in mylonite with varied bimineralic composition and its effect on lithospheric strength. Tectonophysics 303, 175–191]. Our results suggest a dramatic weakening of the bulk rock strength at an early stage of the layer development. We also found that formation of muscovite in the layer structures by breakdown of feldspar can result in further weakening in the layer structure. The bulk-rock strength with mica-bearing layers is reduced by a significant amount, compared with the mica-absent layers. Our analysis suggests that layer development with syntectonic formation of mica can be a major source of weakening for granitic rocks.

Keywords: Weakening; Layer development; Granite; Syntectonic muscovite; Rheology

1. Introduction

The rheology of granitic rocks has a fundamental importance for understanding the mechanical behavior of continental crust since these are the most common rock types that constitute continental crust. Extensive research has been carried out to understand the rheology of granitic rocks at different crustal conditions (e.g. Evans, 1988; Tullis, 1990; Dell'Angelo and Tullis, 1996; Schulmann et al., 1996; Bagdassarov and Dorfman, 1998). One of the common deformation-related features in these rocks is the development of high strain zones due to localization by material weakening (Rutter, 1999) or bifurcation-related system behavior (Hobbs et al., 1990). Development of high strain zones leads to the formation of layered structures. For deformed granitic rocks, the development of layers is a prominent feature at all crustal depths. Banded or striped gneiss of granitic composition is commonly observed in the lower crust (e.g. Schulmann et al., 1996). In the upper crust, development of mica-rich layers formed by breakdown of feldspar is also common (e.g. Evans, 1988). At middle crustal depth, development of composite *S–C* foliation is common (e.g. Lister and Snoke, 1984; Shimamoto, 1989). As layers develop in granitic rocks, the strength of the rocks also changes due to changes in geometric arrangement of constituent minerals. Thus, the strength of granitic rocks can be strain-dependent if layer structures develop as strain accumulates. In recent studies, strain-dependent strength has been formulated for mica-rich rocks where the onset of dynamic recrystallization marks the strength drop (Rutter, 1999).

In this study, we try to quantify a strain-dependent flow law by integrating the end-member flow laws of Handy et al. (1999). Our work can be applied to mid-crustal granitic rocks that deform by crystal plasticity of quartz and cataclasis of feldspar. We also provide a natural example of layer development in granitic rocks deformed in the middle crust and discuss how strength changes of the bulk rock result in changes in deformation mechanisms.

* Corresponding author
E-mail address: youngdo.park@gmail.com (Y. Park).
[1] Present address: Research Division, Heesong Geotek Co. Ltd, Yoonhwa Building, 16-3 Yangjae-dong, Seocho-ku, Seoul 137-888, Korea.

0191-8141/$ - see front matter © 2006 Elsevier Ltd. All rights reserved.
doi:10.1016/j.jsg.2006.02.005

2. Layer development in deforming granitic rocks: an example from the Yecheon shear zone

An example of layer development in deformed granitic rocks is described in this section. The deformed granitic rocks occur in the Yecheon shear zone of central Korea (Fig. 1). The Yecheon shear zone is a branch of the middle Jurassic Honam shear zone system, which is an important tectonic element in forming the current geology of Korea (Ree et al., 2001). An excellently exposed outcrop of about 200 m in length occurs near the central part of the shear zone (AB in Fig. 1). A northeast-striking mylonitic foliation and southwest-trending lineation with a shallow plunge angle are developed in the shear zone (Fig. 1). Local curvature of foliation in weakly deformed rocks as well as other microstructural criteria including oblique grain-shape foliation of recrystallized quartz, asymmetric microfolds of mylonitic layers, mica fish and antithetic microfaults of fractured feldspar grains consistently indicates a dextral sense of shear. We interpret the current exposure of the shear zone as representing a middle crustal section of the Jurassic shear zone, based on the timing and depth of emplacement of the granite protolith for the deformed granitic rocks in the shear zone margin. The emplacement timing of the granite protolith is close to the deformation age of the shear zone (Kwon and Ree, 1997; Otoh et al., 1999), and the depth condition for the deformation should be close to the emplacement depth (about 10–15 km based on hornblende Al geobarometry) for the granites (Cho and Kwon, 1994).

The granitic rocks in the Yecheon shear zone are mainly composed of quartz (30%), K-feldspar (35%), and plagioclase (30%) with minor amounts of muscovite and opaque minerals. The modal percentage of the constituent phases was determined optically with scan lines. For samples with fine grain size (10∼50 μm) in highly deformed rocks, thin sections with thickness of ∼10 μm were prepared so that grain- and phase-boundaries become discernible for optical determination of modes. The granitic rocks show various stages of layer development during mylonitization (Fig. 2). The observed mylonitization can be divided into three stages: (1) a weakly deformed stage where layers of recrystallized quartz grains start to form (Fig. 2a), (2) an intermediate stage where layers of recrystallized quartz grains form a linked network (Fig. 2b and c), and (3) a highly deformed stage where layers constitute most of the rock volume (Fig. 2d).

The weakly deformed granites are composed of about 65% feldspar, 30% quartz, and 5% accessory minerals. Feldspars with a grain size of 0.4–2.5 mm constitute a load-bearing framework, while quartz occupies interstices between feldspars (Fig. 2a). This structure is comparable with the load-bearing framework (LBF) structure of Handy (1990). Feldspar microstructure is characterized by intergranular or intragranular fractures oriented at high angles to the shear zone boundary (Fig. 2a). Patchy and sweeping undulose extinction is

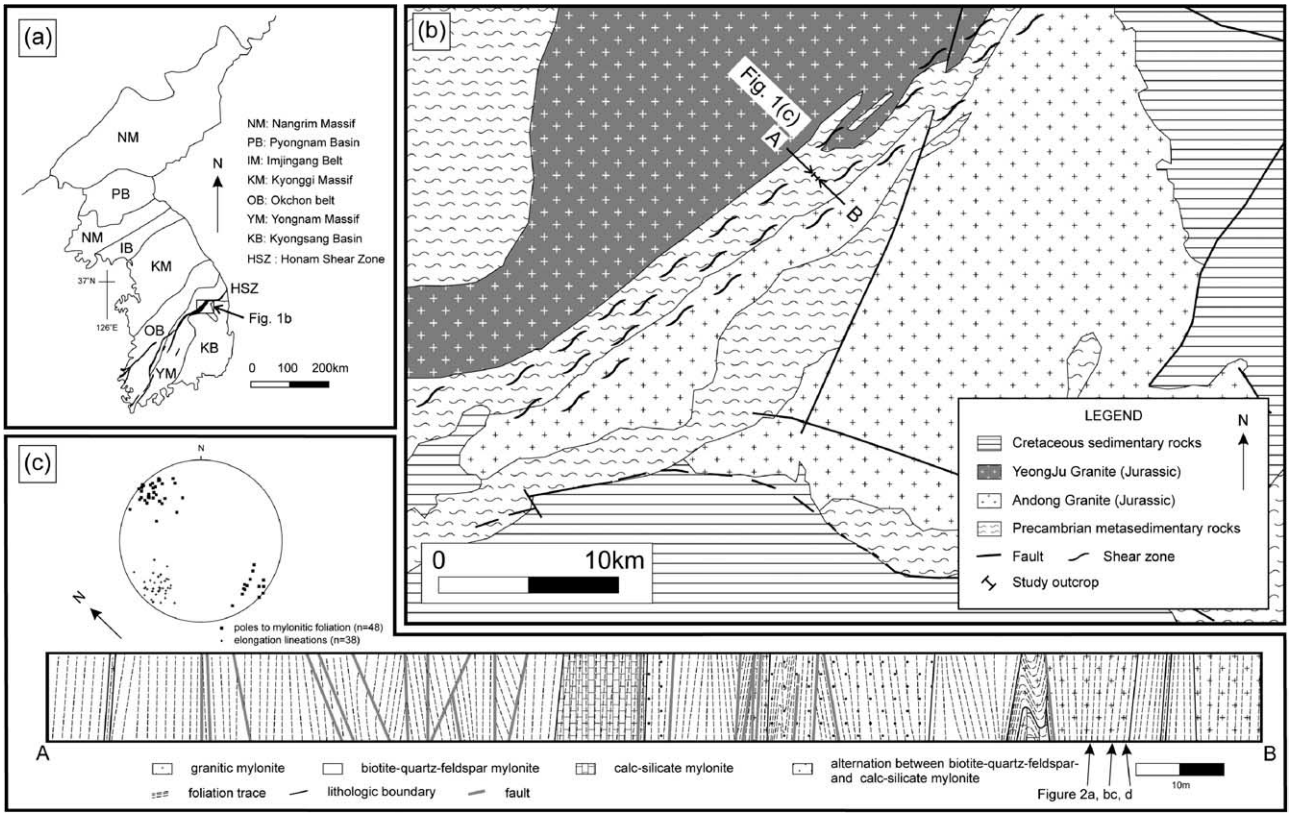

Fig. 1. (a) Tectonic province map of Korea. (b) Geologic map of the Yecheon shear zone (modified after Hwang et al., 2002). (c) Detailed geologic map of the outcrop and orientation data of mylonitic foliation and lineation. Arrows indicate sample localities.

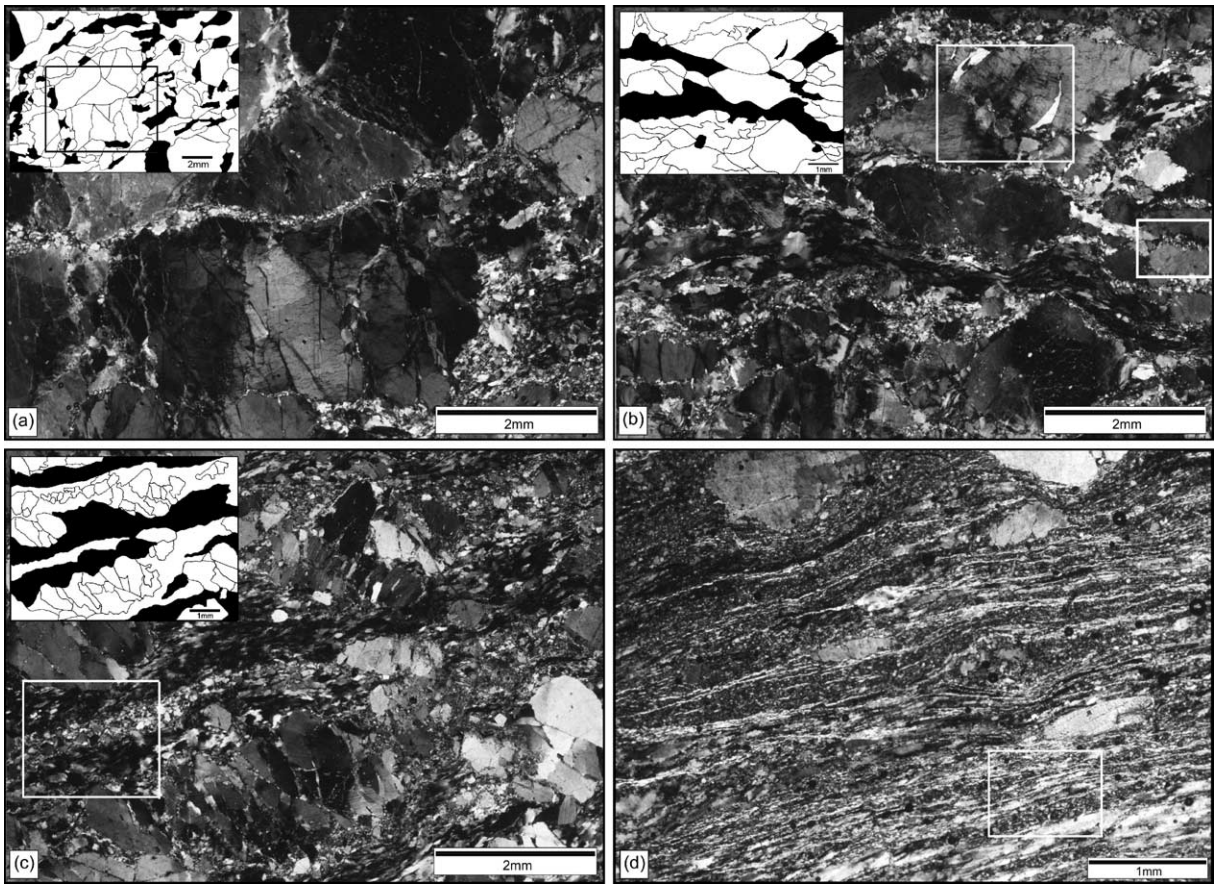

Fig. 2. Layer development in the granitic rocks of the Yecheon shear zone. Thin sections were cut perpendicular to the mylonitic foliation and parallel to the elongation lineation (longer edges of the photomicrographs). (a) Weakly deformed stage. (b) and (c) Intermediate stage. (d) Highly deformed stage. All photomicrographs were taken under crossed-polarized light. Inset: white area and dark area indicate framework feldspar and layered aggregates of feldspar and quartz, respectively.

also observed in some feldspar grains. Some fine feldspar grains with 20–80 μm in size start to form at grain or phase boundaries. In contrast to feldspar, which deforms cataclastically, crystal plasticity is the dominant deformation mechanism for quartz. Quartz grains are slightly elongated and they show patchy or sweeping undulose extinction. Some dynamically recrystallized fine grains occur mainly along boundaries between adjacent quartz grains. In summary, the deformation of feldspar is dominated by fracturing with a minor role of crystal plasticity, whereas quartz deforms by crystal plasticity together with the surrounding deforming feldspar framework. Thus, the deformation of the granitic rock at this stage is governed by the framework feldspar grains that deform by fracturing.

The deformed granitic rocks at the intermediate stage are characterized by the development of interconnected layers consisting of recrystallized quartz, and fractured and some recrystallized feldspar-rich layers (Fig. 2b and c). Thus, the formation of layers involves dynamic recrystallization of quartz and disintegration of feldspar by cataclasis and minor recrystallization. The deformed rocks at the intermediate stage consist of feldspar (55%), quartz (30%), mica (10%), and minor components (5%). Fine feldspar grains occurring between the host feldspar grains have two different origins. Relatively larger (up to ~200 μm) feldspar grains with angular shapes (Fig. 3a) tend to have the chemical compositions identical to those of the host feldspar grains. These grains are interpreted to have a fracture origin (Tullis and Yund, 1987). On the other hand, feldspar grains with finer grain size (~20 μm; Fig. 3b) have chemical compositions of albite ($Na_2O/K_2O = 50 \sim 200$ in wt.%), which is very different from the compositions of host K-feldspar grains ($Na_2O/K_2O = 0.02 \sim 0.04$ in wt.%). This suggests that these fine-grained feldspars are neocrystallized grains formed by chemical breakdown of host feldspar grains, as observed in mid-crustal granitic mylonites (Fitz Gerald and Stünitz, 1993). The wavy or lobate boundaries between the fine and the host feldspar grains are also observed. This suggests that there may have been a migration of phase boundaries between them during and/or subsequent to neocrystallization of albite. Thus, it is interpreted that fracturing and neocrystallization along fracture planes contributed to the formation of fine-grained feldspars. Formation of muscovite by breakdown of feldspar (O'Hara, 1988; Fitz Gerald and Stünitz, 1993) is also recognized in places where fine-grained feldspar grains are present. O'Hara (1988) suggested the following two reactions for forming muscovite in granitic rocks:

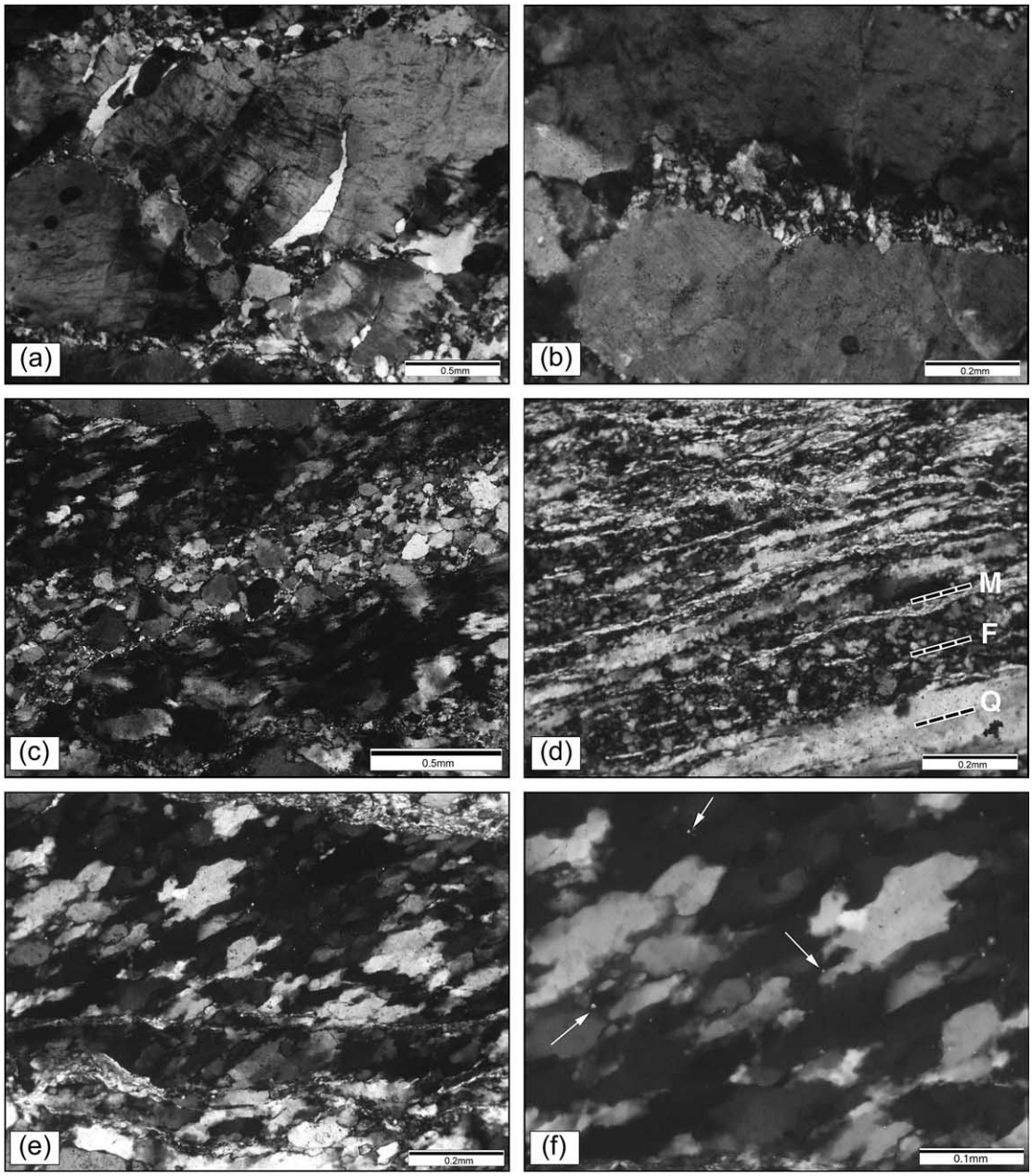

Fig. 3. Microstructures of feldspar and quartz. (a) Fractured feldspar at the intermediate stage (enlarged view of the upper white box in Fig. 2b). (b) Aggregates of fractured feldspar grains with minor dynamic recrystallization along the fracture at the intermediate stage (enlarged view of the lower white box in Fig. 2b). (c) Alternating layers of feldspar and quartz aggregates at the intermediate stage (enlarged view of Fig. 2c). (d) Alternating layers of feldspar (F), quartz (Q), and mica (M) aggregates at the highly deformed stage (enlarged view of Fig. 2d). (e) Quartz microstructure at the highly deformed stage. (f) The secondary phase particle (arrows) at grain boundary of quartz at the highly deformed stage.

$$3\mathrm{K-feldspar} + \mathrm{H_2O} = \mathrm{muscovite} + 6\mathrm{SiO_2} + \mathrm{K_2O}$$

$$4\mathrm{oligoclase} + 6\mathrm{K-feldspar} + \mathrm{K_2O} + 9\mathrm{H_2O} = 2\mathrm{zoisite} + 8\mathrm{muscovite} + 44\mathrm{SiO_2} + 8\mathrm{Na_2O}$$

The increased surface to volume ratio due to fracturing of feldspar may have facilitated the muscovite-forming reaction. Most of the mica grains occur along intragranular fractures of feldspar grains, although some mica-rich layers begin to develop parallel to mylonitic foliation (Fig. 2b).

Two types of quartz microstructures are observed: (1) fracture-filling quartz, and (2) quartz within interconnected layers. Fig. 3a shows quartz veins that fill fractures in feldspar. This suggests precipitation of quartz and other minerals from solution. Some portions of fine-grained quartz (Fig. 3e) may also have a precipitation origin (e.g. Shimamoto et al., 1991). Thus, it is interpreted that dissolution and precipitation may have contributed to total deformation. Most quartz grains in the interconnected layers show a strong lattice preferred orientation, sweeping undulose extinction, elongated ribbon grains

including subgrains, and deformation lamellae. Locally, some quartz layers between relatively large feldspar grains form extremely elongated ribbon grains (aspect ratio of 1:7∼8). Near the boundaries of these elongated quartz grains, fine recrystallized grains are generally observed. The recrystallized fine grains are about the same size as subgrains, suggesting that dynamic recrystallization by progressive rotation of subgrains is dominant (Urai et al., 1986; Hirth and Tullis, 1992; Passchier and Trouw, 1996). These microstructures are characteristic of dislocation creep regime II of Hirth and Tullis (1992) where rotational recrystallization is a dominant recovery process.

The phase distribution at the highly deformed stage is characterized by quartz-rich, feldspar-rich, and muscovite-rich layers, so that all of the phases constitute interconnected layers (Figs. 2d and 3d). This structure is comparable with the interconnected weak layer (IWL) structure of Handy (1990). In the quartz-rich layer, quartz ribbons of dynamically recrystallized aggregates show sweeping undulose extinction and subgrains (Fig. 3e). The recrystallized quartz grains within the ribbons also show a grain-shape foliation oblique to the flow direction (Fig. 3e). The boundaries of adjacent quartz grains are generally wavy and lobate (Fig. 3e), indicating grain boundary migration recrystallization. Very fine grains of second-phase particles with a size of less than a few μm occur at the wavy boundaries of quartz, indicating impurity-controlled grain boundary migration (Urai et al., 1986) (Fig. 3f). These microstructures are thought to be characteristic of the transition between dislocation creep regimes II and III of Hirth and Tullis (1992). In feldspar-rich layers, on the other hand, the fine, irregular-shaped feldspars, mostly 10–50 μm in size, show no grain shape-preferred orientation (Fig. 3d). In muscovite-rich layers, fine-grained muscovites are generally aligned parallel or sub-parallel to the flow plane (Fig. 3d). The volume fraction of the constituent phases in this state is also different from that in weakly deformed state; the rocks consist of about 30% quartz, 40% feldspar, and 25% muscovite, with 5% of minor components, indicating that there is a significant increase in muscovite content. The syntectonic breakdown reaction of feldspar is responsible for the increase in muscovite content and possibly for the strength decrease of the bulk rock as well.

3. Strength changes during layer development

We have described a mid-crustal example of layer development in granitic rocks from a natural shear zone. As the layers that consist of fine grained feldspar and quartz form, the rheology of the granitic rocks changes from framework-controlled to layer-controlled. Handy (1994) and Handy et al. (1999) suggested flow laws for bi-mineralic rocks with two end-member textures or phase distribution: (1) load-bearing framework (LBF); when the volumetrically larger phase forms a framework structure, the framework becomes stress-supporting. Thus, the strength of the bi-mineralic rock is controlled by the strength of the framework. (2) Interconnected weak layer (IWL); when the weaker phase forms layers, much of the strain is concentrated in the weaker layers. Thus, the rheology of the rock is controlled by the strength of the weaker-phase layers with IWL geometry. Here, we will combine the end-member flow laws by mixing the end-member geometries of phase distribution, and then we will investigate how the strength of granitic rocks changes with time when layers develop. In our analyses of flow laws, we consider the quartz- and feldspar-rich layers only. The effect of mica-rich layers will be discussed later. A schematic diagram for the combined flow laws is shown in Fig. 4.

3.1. End-member flow laws for LBF and IWL structures

The end-member flow laws developed by Handy et al. (1999) are adopted here. The brittle strength of feldspar is considered for the strength of the LBF structure, because we are interested in the property of the granitic rocks near the middle crustal level. Since the stronger phase, feldspar, deforms largely by frictional flow including microcracking, frictional sliding, and rotation, the strength of feldspar can be taken from the Coulomb criterion for frictional flow (Streit, 1997) (see Table 1 for the details of the symbols).

$$\tau_s = \frac{1}{2}[a + P_{\text{eff}}(b-1)\sin(90 - \arctan\mu_d)] \quad (1)$$

The term, a in the above equation is related to the critical shear strength, t_0 (see Table 1). Since the critical shear strengths are different between intact feldspar and feldspar aggregates, it is desirable to use different values for t_0, but we used the same values for the two conditions. Thus, our analysis of strength for IWL structure (discussed later) will result in higher strength of feldspar-aggregate layers because the critical shear strength of intact feldspar is higher than that of feldspar aggregates.

For the case of IWL structure, the flow strength depends largely on volume fraction and strength contrast between constituent phases. The strength of the IWL structure is expressed with the equation (Eq. 5 of Handy et al., 1999):

$$\tau_r^{\text{IWL}} = \tau_w \phi_w^{1/\tau_c} + \tau_s(1 - \phi_w^{1/\tau_c}) \quad (2)$$

The flow strength of the weak phase can be approximated with the experimentally inferred power law of quartzite (Eq. 1 of Hirth et al., 2001). It is also assumed that the weaker phase, quartz, deforms by dislocation creep.

$$\dot{\varepsilon} = A f_{H_2O}^m \tau_w^n \exp(-Q/RT) \quad (3)$$

In summary, the strength of the LBF structure for the granitic rocks at the middle crustal level is obtained from the frictional strength of the feldspar using Eq. (1). For the IWL structure, the strength can be obtained from Eq. (2) using the brittle strength of feldspar (Eq. (1)) and the flow stress of quartz (Eq. (3)).

3.2. Choice of parameters and assumptions for strength calculations

We assumed 300 °C and 400 MPa as representing the middle crustal condition (i.e. 15 km depth condition with 20 °C km^{-1} geothermal gradient and ∼27 MPa km^{-1}

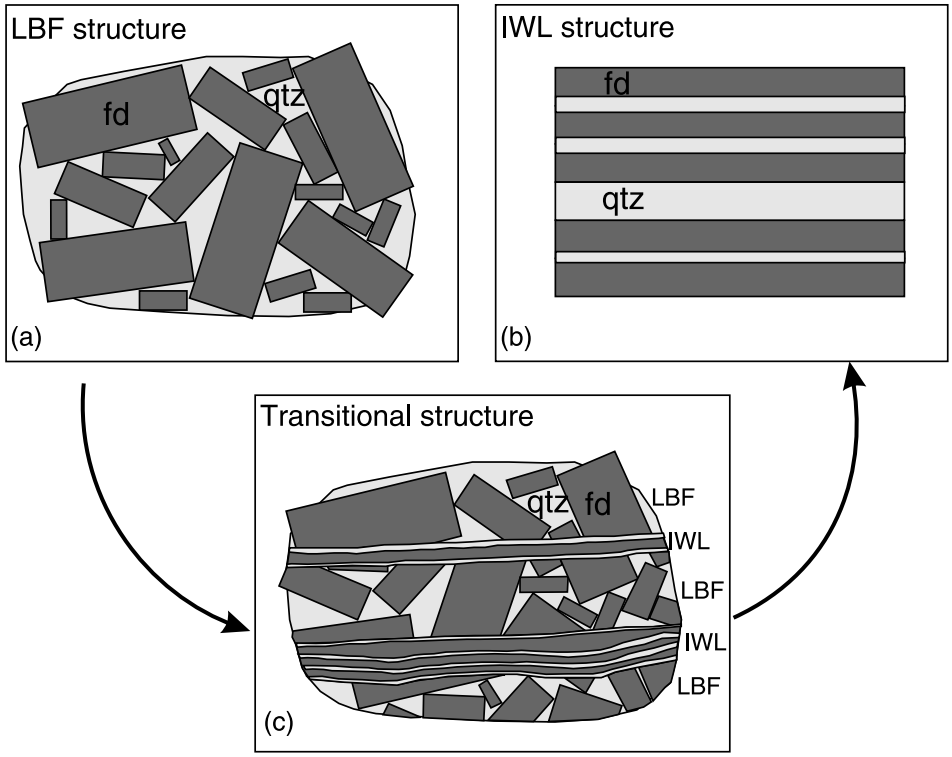

Fig. 4. Schematic phase distribution in granitic rocks (fd: feldspar, qtz: quartz). (a) Load-bearing framework (LBF) structure. (b) Interconnected weak layer (IWL) structure. (c) Transitional structure from LBF to IWL structure

pressure gradient). For the calculation of the strength of feldspar, effective pressure (P_{eff} in Eq. (1) and Table 1) is an important factor. If we assume fluid pressure factor to be 0.8, the fluid pressure will be 320 MPa (0.8×400 MPa). Thus, the effective pressure will be 80 MPa at model conditions (400–320 MPa).

Fluid pressure also affects the ductile strength of quartz through f_{H_2O} term in Eq. (3). If we assume the same fluid pressure factor value (0.8), fluid pressure becomes 320 MPa and f_{H_2O} becomes ~26 MPa (i.e. [fluid pressure factor]× [fugacity coefficient]=320 MPa×0.081, where 0.081=standard water fugacity coefficient at 300 °C; Tödheide, 1972).

Ductile strength of quartz is also rate dependent. Thus, it is necessary to assume strain rate for the estimation of strength. We assumed the strain rate to be $3\times10^{-15}\,s^{-1}$. Effects of strain rate and fluid pressure on bulk strength are discussed later.

3.3. Combined flow law for coexisting LBF and IWL structures

For granitic rocks starting to develop layers, the strength of the bulk rock can be estimated by combining the end-member flow laws derived by Handy et al. (1999):

$$\tau_r^{\text{transition}} = \tau_{\text{IWL}}\phi_{\text{layer}}^{1/\tau_c} + \tau_{\text{LBF}}(1-\phi_{\text{layer}}^{1/\tau_c}) \quad (4)$$

The form of this equation is identical to that of Eq. (2), with a replacement for some terms. Thus, Eq. (4) treats the deforming layered rock as consisting of layers of weaker phases and layers of stronger feldspar framework (Fig. 4c). In other words, in the granitic rocks containing both LBF and IWL structures simultaneously, the local layers or IWL part accommodate most of the strain in the bulk rock and this leads to both strain and strain-rate partitioning as similar to that in the IWL structure (Handy, 1990). The strengths of both LBF and IWL structures for Eq. (4) are calculated from Eqs. (3) and (1), respectively. Calculation of the strength of the bulk rock is straightforward once the volume proportion of the IWL structure is known. Fig. 5a and b shows the plots of volume proportion of the IWL structure vs. strength of the bulk rock for different conditions of fluid pressure and strain rate. It is observed in some conditions that a dramatic decrease in strength occurs at the initial stage of layer development.

4. Discussion

4.1. Strain-dependence of strength

It is shown in Fig. 5 that the strength of granitic rocks is a function of the volume fraction of the IWL structure (Eq. (4)). Although the IWL volume fraction–strength relation is straightforward, there are difficulties in estimating the strength of deforming granitic rocks. This is because the relation between strain and volume proportion of the IWL is not clearly known. Once the strain–IWL volume relation is established, it is possible to expand the results (e.g. Fig. 5b) to geologically more meaningful strain–strength relations. In this section, we will examine how the IWL volume increases with strain.

Table 1
Rheological parameters in the equations of text

Eq. no.	Parameters and constants		Values used for calculation
(1)	$\tau_s = \frac{1}{2}[a + P_{eff}(b-1)\sin(90 - \arctan\mu_d)]$		
	τ_s	Strength of material undergoing frictional sliding (MPa)	
	μ_d	Coefficient for dynamic friction	0.6 (Byerlee, 1978)
	b	$\{(1+\mu_d^2)^{1/2}\mu_d\}^{-2}$	
	t_0	Critical shear strength	50 MPa (Byerlee, 1978)
	a	$2\cdot t_0 \cdot b^{1/2}$	
	P_{eff}	Effective pressure (MPa)	80 MPa (see text for details)
(2)	$\tau_r^{IWL} = \tau_w \phi_w^{1/\tau_c} + \tau_s(1-\phi_w^{1/\tau_c})$		
	τ_r^{IWL}	Bulk rock strength of biphase rocks with interconnected weak layer structure (MPa)	
	τ_w	Strength of weaker phase	
	τ_s	Strength of stronger phase	
	ϕ_w	Volume fraction of weak phase	
	τ_c	Strength ratio ($=\tau_s/\tau_w$)	
(3)	$\dot{\gamma} = A f_{H_2O}^m \tau_w^n \exp(-Q/RT)$		
	$\dot{\gamma}$	Strain rate (s^{-1})	3×10^{-15} s^{-1}
	A	Pre−exponential term	$10^{-11.2}$ MPa^{-n} s^{-1} (Luan and Paterson, 1992)
	f_{H_2O}	Water fugacity	25.92 MPa (Tödheide, 1972)
	m	Water fugacity exponent	1 (Hirth et al., 2001)
	τ_w	Strength (MPa) of weaker phase	
	N	Power-law exponent	4 (Luan and Paterson, 1992)
	Q	Activation energy	135,000 J mol^{-1} (Luan and Paterson, 1992)
	R	Universal gas constant	8.3144 J K^{-1} mol^{-1}
	T	Absolute temperature	K
(4)	$\tau_r^{transition} = \tau_{IWL}\phi_{layer}^{1/\tau_c} + \tau_{LBF}(1-\phi_{layer}^{1/\tau_c})$		
	$\tau_r^{transition}$	Bulk rock strength of biphase rocks at transitional state from LBF to IWL structure (MPa)	
	τ_{IWL}	Strength of part in biphase rocks with IWL structure	
	τ_{LBF}	Strength of part in biphase rocks with LBF structure	
	ϕ_{IWL}	Volume fraction of IWL structure	
	τ_c	Strength ratio ($=\tau_{IWL}/\tau_{LBF}$)	
(5)	$\dot{\gamma}_{layer} = \dot{\gamma}_{bulk\ rock}\phi_{layer}^{1/\tau_c - 1}$		
	τ_c	Strength contrast (or ratio) ($=\tau_s/\tau_w$)	
	τ_s	Strength of stronger phase	
	τ_w	Strength of weaker phase	
	$\dot{\gamma}_{layer}$	Strain rate (s^{-1}) of interconnected layers	
	$\dot{\gamma}_{bulk\ rock}$	Strain rate (s^{-1}) of bulk rock	
	ϕ_{layer}	Volume proportion of interconnected layers	

In fault gouge experiments where new particles are generated by cataclasis, it is known that the particle size distribution obeys the power-law function, $N(n)/A = bn^{-D}$, where $N(n)$ is the number of particles of a certain size range, A is the area examined, n is the mean size for the size range from which frequency $N(n)$ is counted, b is a constant, and D is also a constant representing the fractal dimension (Sammis et al., 1987). Theoretically, the value of D for fault gouge is known to be 2.58 (Sammis et al., 1987).

Experiments of simulated fault gouge with increasing shear strain show that the fractal dimension, D, of the particle distributions undergoes a rapid initial increase and gradually approaches the value of about 2.6 at a shear strain of about 1.5 (see fig. 11 in Marone and Scholz, 1989), and thus the experimental steady-state D value is close to the theoretical one. This implies that the mean particle size is inversely related to shear strain; a rapid initial decrease and then gradual decrease with strain. The experimental results imply that generation of smaller particles is prominent at low strain, the rate of generation becomes slower with strain, and finally reaches a steady state. We think that the fault gouge experiment may be analogous to development of layers in granitic rocks because at least one important process (fracturing of feldspar), among many processes, is similar to fracturing in the gouge experiments. Thus, we assumed rapid increase in IWL volume fraction at small strain and slower increase over time (inset of Fig. 5c). However, the shear strain value of 1.5, when the fractal dimension reaches a steady state (Marone and Scholz,

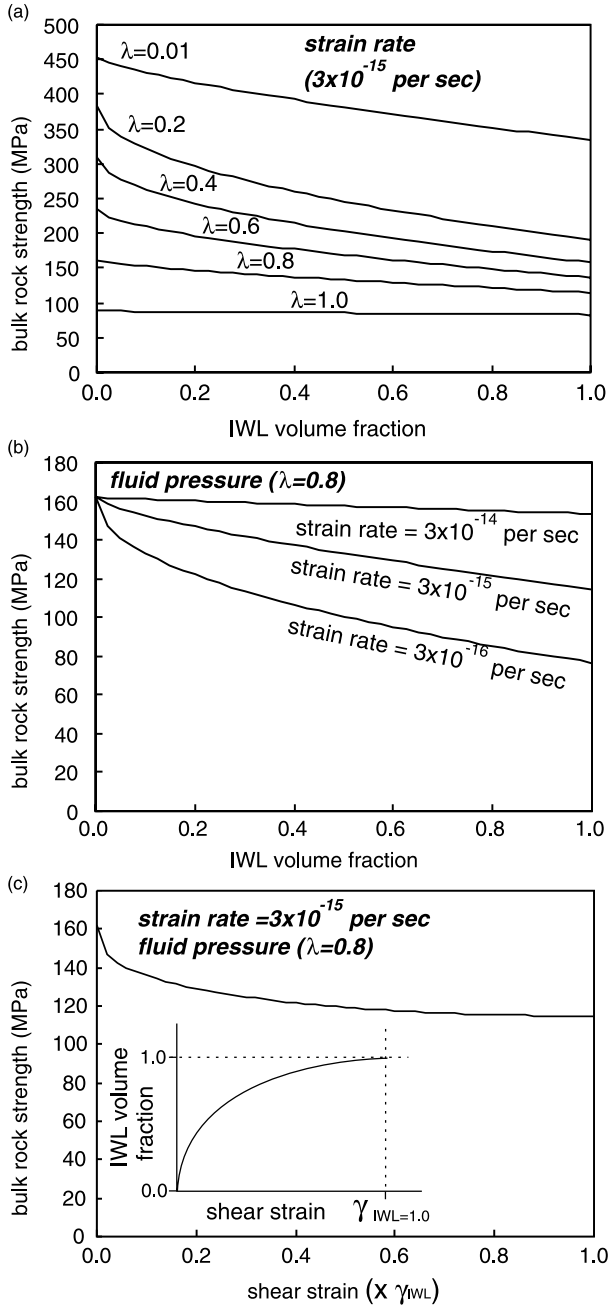

Fig. 5. Changes in bulk-rock strength as a function of IWL volume fraction and strain. (a) Changes in strength for different fluid pressure conditions. (b) Changes in strength for strain-rate conditions. (c) Changes in strength with strain. See text for details.

1989), may not be universal because the behavior of fracturing is material dependent. Therefore, it is difficult to predict precisely how strength changes with strain. However, we can still predict that strength decrease is most prominent during the initial stage of layer development. Fig. 5c shows the strain–strength relation with assumed strain–IWL volume fraction relation (inset of Fig. 5c). Dramatic strength decrease is shown due to a rapid increase in IWL volume fraction at the initial stage of deformation.

The effect of fluid pressure on strength changes in rocks with layer structures is investigated for a constant strain-rate condition. Fig. 5a shows how fluid pressure affects the strength with development of layer structures. The decrease in strength in Fig. 5a is more prominent when fluid pressure is lower. For higher fluid conditions, strength drop occurs by a smaller amount. Fluid pressure affects both the brittle strength of feldspar and the ductile strength of quartz. When fluid pressure is lower, weakening occurs with development of quartz-rich layers. However, when fluid pressure is higher, feldspar also becomes weaker so that the strength contrast between feldspar and quartz becomes smaller. In this case, the effect of development of quartz-rich layers becomes smaller in lowering the bulk rock strength.

We also investigated how strain rate affects the strength of rocks with layer structures while fixing the value of fluid pressure (Fig. 5b). More significant weakening is observed for lower strain rates. This is due to the response of ductile quartz to strain rate. Unlike fluid pressure, strain rate affects only the strength of quartz since the Mohr–Coulomb behavior of feldspar is rate insensitive. Thus, when higher strain rate is imposed, quartz becomes stronger, and this will result in stronger IWL compared with the strength of IWL for lower strain rate. In this case, weakening by smaller degree occurs.

4.2. Transition in deformation mechanisms and changes in shear-zone strain rate during layer development

At the intermediate or highly deformed stages, when layered structures develop, strain rate is not homogeneous within rocks due to the difference in strength of the layers. The degree of strain-rate ($\dot{\gamma}$) partitioning within rocks depends largely on the strength contrast ($\tau_c = \tau_s/\tau_w$) between phases and volume proportion (ϕ_{layer}) of interconnected layers (Handy, 1994).

$$\dot{\gamma}_{layer} = \dot{\gamma}_{bulk\ rock}\phi_{layer}^{1/\tau_c - 1} \tag{5}$$

We can interpret the above equation in two ways: (1) for a shear zone with constant strain rate (i.e. wall rock with constant velocity), and (2) for a shear zone bounded by wall rock that

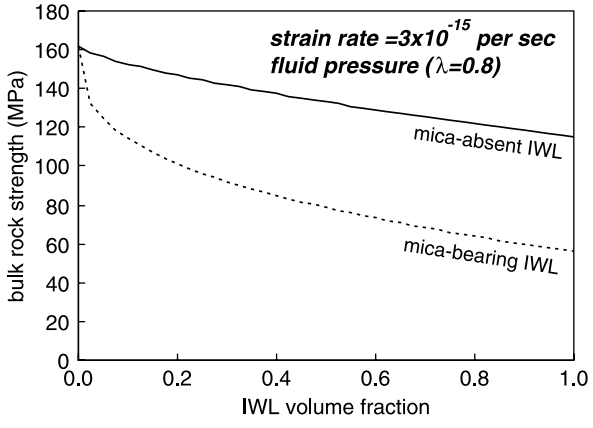

Fig. 6. Changes in bulk-rock strength as a function of IWL volume fraction in mica-absent and mica-bearing IWL.

Table 2
Flow law parameters for the calculation of strength for mica-bearing rocks

	Parameters and constants	Values used for calculation
α	Term related to material property	0.55 MPa^{-1}
C	Term related to material property	1.4×10^{-10} s^{-1}
Q	Activation energy	89 KJ mol^{-1}
R	Universal gas constant	8.3144 J K^{-1} mol^{-1}

For flow law, $\dot{\varepsilon} = C\exp(\alpha\sigma)\exp(-Q/RT)$, refer to Shea and Kronenberg (1992). Temperature and strain-rate for calculation: 300 °C and 3×10^{-15} s^{-1}.

can change velocity. For case (1) where the wall rock moves at constant velocity, strain rate in interconnected layers is inversely related to volume fraction of interconnected layers. Thus, strain rate in quartz-rich layers decreases exponentially as the volume proportion of the layers increases with microstructural transition, and this will result in a transition in deformation processes. In the granitic rocks described earlier, quartz shows a transition in deformation processes as the granitic protolith becomes mylonitic. The major recovery process of quartz is rotational recrystallization (regime II of Hirth and Tullis, 1992) at weakly deformed to intermediate stage (Fig. 2), whereas it is grain-boundary migration recrystallization (with impurity-controlled migration) in addition to rotational recrystallization (transition between regimes II and III) at the highly deformed stage. It is suggested by Hirth and Tullis (1992) that the observed transition occurs with a decrease in strain rate or with an increase in temperature, resulting in a decrease in strength. Thus, we can interpret that the observed microstructural change is related to the changes in deformation processes resulting from the increase in the volume proportion of the layer structure.

When a shear zone is bounded by wall rocks with changing velocity, the $\dot{\gamma}_{layer}$ term in Eq. (5) can increase as the quartz initially surrounded by the framework feldspar becomes unconstrained as the layer structure develops. Then the bulk strain rate would increase as strain localization occurs in the layers. However, we were not able to observe this possibility in our rocks (i.e. transition in deformation mechanism of quartz from lower to higher strain-rate regimes).

In our analyses of the strength of the deforming granitic rocks at mid-crustal level, we assumed a frictional cataclastic flow in the feldspar-rich layers. However, if a viscous granular flow occurs in the feldspar-rich layers with a lower strain rate as demonstrated by Stünitz and Fitz Gerald (1993) in mid-crustal granitic mylonites, the strength of the feldspar-rich layers can be weaker than that of quartz-rich layers. If this is the case, we need a modification of Eq. (1) by incorporating the viscous granular flow law of the feldspar-rich layers.

4.3. Effect of mica-forming reaction

So far, we have considered weakening by textural changes or changes in geometric arrangement of the constituent phases. However, when syntectonic breakdown of feldspar into muscovite occurs (e.g. highly deformed rocks in our example; Figs. 2d and 3d), we can expect that mica-forming reaction would result in further weakening since the strength of mica is known to be weaker than that of quartz and feldspar (Kronenberg et al., 1990; Shea and Kronenberg, 1993). We have explored this possibility with the similar steps discussed above. The IWL part in highly deformed rocks consists of 30% quartz, 40% feldspar, and 25% muscovite (32% quartz, 42% feldspar, and 26% muscovite when recast to 100% total). We assumed that syntectonic breakdown of feldspar occurs from the onset of layer formation (i.e. the modal percentage described above remains constant in the layers). For the estimation of the strength of the IWL layer that consists of quartz, feldspar, and muscovite, we performed two-step calculations using Eq. (2). First, we calculated the strength of the layer of quartz and muscovite. Then, we estimated the strength of the layer of feldspar and mixed layers of quartz and muscovite. It is shown in Fig. 6 how strength changes with the formation of mica-bearing layers (details of strength calculation is in Table 2). The rheology of mica aggregates is estimated from mechanical data of mica–quartz schist ($\sim$75% of mica; Shea and Kronenberg, 1992). Compared with bulk-rock strength with mica-absent layers, the bulk-rock strength with mica-bearing layers decreases more significantly as layer formation proceeds. Thus, mica-forming reaction is interpreted to lower the strength of granites by a significant amount.

5. Conclusions

(1) Granitic rocks from the Yecheon shear zone deformed at middle crustal depths are characterized by development of layer structures with fine grain size, as mylonitization progresses. Dynamic recrystallization of quartz and disintegration of feldspar by fracturing and by neocrystallization lead to formation of fine-grained aggregates, and translation of fine grains develops layer structures in these rocks.
(2) The flow strength of middle crustal granitic rocks with layer structures can be estimated by combining the IWL- and LBF-two-phase flow laws developed by Handy et al. (1999). The combined flow law suggests dramatic weakening at the onset of layer development.
(3) When the strain rate of the shear zone remains constant (i.e. wall rocks moving at constant velocity), transition in quartz deformation processes occurs toward lower strain rate (e.g. toward regime III of Hirth and Tullis (1992)) as the volume fraction of layer structures increases. However, when the strain rate of a shear zone is not constrained, the increase in volume fraction of layer structures can also result in transition in quartz deformation processes toward

higher strain-rate regime. This is because the quartz in the layer may become unconstrained by feldspar and deform faster than the quartz in the feldspar framework.

(4) Formation of mica in the layer structures by syntectonic breakdown of feldspar can result in further weakening in the IWL structure. The bulk-rock strength with mica-bearing layers is reduced by a significant amount, compared with that of the mica-absent layers. Thus, mica-forming reaction can be a major source of weakening mechanism for rocks with granitic compositions.

Acknowledgements

We thank Paul Bons and Toshi Shimamoto for providing thoughtful reviews which improved the paper significantly. We are also appreciative to Richard Norris for editorial handling and Sunghee Choi for microprobe analyses. This work was supported by a grant from Korea Research Foundation (KRF-2000-015-DP0430).

References

Bagdassarov, N., Dorfman, A., 1998. Granite rheology; magma flow and melt migration. Journal of the Geological Society London 155, 853–862.

Byerlee, J., 1978. Friction of rocks. Pure and Applied Geophysics 116, 615–626.

Cho, D.-L., Kwon, S.-T., 1994. Hornblende geobarometry of the Mesozoic granitoids in South Korea and the evolution of crustal thickness. Journal of Geological Society of Korea 30, 41–61 (in Korean with English abstract).

Dell'Angelo, L.N., Tullis, J., 1996. Textural and mechanical evolution with progressive strain in experimentally deformed aplite. Tectonophysics 256, 57–82.

Evans, J.P., 1988. Deformation mechanisms in granitic rocks at shallow crustal levels. Journal of Structural Geology 9, 437–444.

Fitz Gerald, J.D., Stünitz, H., 1993. Deformation of granitoids at low metamorphic grade. I: Reactions and grain size reduction. Tectonophysics 221, 269–297.

Handy, M.R., 1990. The solid-state flow of polymineralic rocks. Journal of Geophysical Research 96, 8647–8661.

Handy, M.R., 1994. Flow laws for rocks containing two non-linear viscous phases: a phenomenological approach. Journal of Structural Geology 16, 287–301.

Handy, M.R., Wissing, S.B., Streit, L.E., 1999. Frictional-viscous flow in mylonite with varied bimineralic composition and its effect on lithospheric strength. Tectonophysics 303, 175–191.

Hirth, G., Tullis, J., 1992. Dislocation creep regimes in quartz aggregates. Journal of Structural Geology 14, 145–159.

Hirth, G., Teyssier, C., Dunlap, W.J., 2001. An evaluation of quartzite flow laws based on comparisons between experimentally and naturally deformed rocks. International Journal of Earth Sciences 90, 77–87.

Hobbs, B.E., Muhlhaus, H.-B., Ord, A., 1990. Instability, softening and localization of deformation. In: Knipe, R.J., Rutter, E.H. (Eds.), Deformation Mechanisms, Rheology and Tectonics. Geological Society, London, Special Publications 54, pp. 43–165.

Hwang, S.K., Chang, T.W., Kim, J.M., Ahn, U.S., Lee, B.H., 2002. Lithofacies and multiphase emplacement in the Andong batholith. Journal of Geological Society of Korea 38, 51–65 (in Korean with English abstract).

Kronenberg, A.K., Kirby, S.H., Pinkston, J., 1990. Basal slip and mechanical anisotropy of biotite. Journal of Geophysical Research 95, 19207–19278.

Kwon, S.-T., Ree, J.-H., 1997. A note on the age of the Honam Shear Zone. Journal of Geological Society of Korea 33, 183–188 (in Korean with English abstract).

Lister, G.S., Snoke, A.W., 1984. S–C mylonites. Journal of Structural Geology 6, 617–638.

Luan, F.C., Paterson, M.S., 1992. Preparation and deformation of synthetic aggregates of quartz. Journal of Geophysical Research 97, 301–320.

Marone, C., Scholz, C.H., 1989. Particle-size distribution and microstructures within simulated fault gouge. Journal of Structural Geology 11, 799–814.

O'Hara, K., 1988. Fluid flow and volume loss during mylonitization: an origin for phyllonite in an overthrusting setting, North Carolina, U.S.A.. Tectonophysics 156, 21–36.

Otoh, S., Jwa, Y.J., Nomura, R., Sakai, H., 1999. A preliminary AMS (anisotropy of magnetic susceptibility) study of the Namwon granite, southwest Korea. Geosciences Journal 3, 31–41.

Passchier, C.W., Trouw, R.A.J., 1996. Microtectonics. Springer-Verlag, Berlin.

Ree, J.-H., Kwon, S.-H., Park, Y., Kwon, S.-T., Park, S.-H., 2001. Pretectonic and posttectonic emplacements of the granitoids in the south central Okchon belt, South Korea: implications for the timing of the strike-slip shearing and thrusting. Tectonics 20, 850–867.

Rutter, E.H., 1999. On the relationship between the formation of shear zones and the form of the flow law for rocks undergoing dynamic recrystallization. Tectonophysics 303, 147–158.

Sammis, C.G., King, G., Biegel, R., 1987. The kinematics of gouge deformation. Pure and Applied Geophysics 125, 777–812.

Schulmann, K., Mlcoch, B., Melka, R., 1996. High-temperature microstructures and rheology of deformed granite, Erzgebirge, Bohemian Massif. Journal of Structural Geology 18, 719–733.

Shea, W.T., Kronenberg, A.K., 1992. Rheology and deformation mechanisms of an isotropic mica schist. Journal of Geophysical Research 97, 15201–15237.

Shea, W.T., Kronenberg, A.K., 1993. Strength and anisotropy of foliated rocks with varied mica contents. Journal of Structural Geology 15, 1097–1121.

Shimamoto, T., 1989. The origin of S–C mylonites and a new fault-zone model. Journal of Structural Geology 11, 51–64.

Shimamoto, T., Kanaori, Y., Asa, K., 1991. Cathodoluminescence observations on low-temperature mylonites: potential for detection of solution-precipitation microstructures. Journal of Structural Geology 13, 967–973.

Streit, J.E., 1997. Low frictional strength of upper crustal faults: a model. Journal of Geophysical Research 102, 24619–24626.

Stünitz, H., Fitz Gerald, J.D., 1993. Deformation of granitoids at low metamorphic grade. II: Granular flow in albite-rich mylonites. Tectonophysics 221, 299–324.

Tödheide, K., 1972. Water at high temperature and pressure. In: Franks, F. (Ed.), Water: A Comprehensive Treatise. Plenum Press, New York, pp. 463–514.

Tullis, J., 1990. Experimental studies of deformation mechanisms and microstructures in quartzo-feldsparthic rocks. In: Barber, D.J., Meredith, P.G. (Eds.), Deformation Processes in Minerals, Ceramics and Rocks. Unwin Hyman, London, pp. 190–227.

Tullis, J., Yund, R.A., 1987. Transition from cataclastic flow to dislocation creep of feldspar: mechanisms and microstructures. Geology 13, 238–241.

Urai, J.L., Means, W.D., Lister, G.S., 1986. Dynamic recrystallization of minerals. In: Heard, H.C., Hobbs, B.E. (Eds.), Mineral and Rock Deformation: Laboratory Studies—The Paterson Volume. American Geophysical Union, Geophysical Monograph 36, pp. 161–199.